Development of KAGRA Photon Calibrator for Hardware Injection Test

Yu-Kuang Chu

國立臺灣師範大學

Recommended for Acceptance

by the Department of

Physics

Adviser: Wo-Lung Lee

June 2018

Abstract

Abstract

Acknowledgements

Takayuki Tomaru, Nobuyuki Kanda, Yuki Inoue, Takaaki Yokozawa, Takahiro Yamamoto, Darkhan Tuyenbayev, Chihiro Kozakai, Chih-Hsun Lin, Ming-Lee Chu Bin-Hua Hsieh KEK(Emiko Kotaki, Ayako Hagiwara, Ayako Ueda)(Kunihiko Hasegawa, Tomohiro Yamada, Takaharu Shishido, Rishabh Bajpai,) KAGRA(Mihoko Okinaka, Rie Kikuchi)(Takafumi Ushiba, Koki Okutomi, Takahiro Miyamoto and Yutaro Enomoto) ASIOP (Pei-Rong Tsai, Chia-Yi Lee) , Sadakazu Haino, Wolung Lee

To my parents.

Contents

List of Tables

List of Figures

Chapter 1

Introduction

When you got a new camera, you probably will take a lot of testing photos before you start to use it seriously. Similarly, we would like to test our gravitational wave detector before we use it to see the Universe.

Hardware injection test is a process to verify the performance of interferometer by sending sample signals into interferometer[1]. Ideally, we should prepare some real gravitational waves as test signals. But it is practically hard to generate large enough artificial gravitational waves that are detectable by current technology.

Therefore, instead of generating gravitational waves, people mimic the effect of celestial gravitational waves by displacing the mirror according to the simulated gravitational waveforms, changing arm length correspondingly, comparing the optical readout in the main interferometer, thereby checking the response of their interferometer.

Among different ways to push those Test Mass Mirrors in the main interferometer, radiation pressure of external laser beams have been used because its simplicity and stability. A dedicated auxiliary laser system called Photon Calibrator(PCal) has been developed for this purpose.

In this dissertation, I will briefly explain what is photon calibrator and how it works for calibration and hardware injection purposes. Then, I will discuss the noise

problem from current signal generating system that is used to control PCal Laser intensity. Finally, a possible solution, Analog De-Whitening Filter, has been manufactured and tested with Photon Calibrator in Kamioka Gravitational Wave Detector (KAGRA).

1.1 Introduction to Gravitational Wave

1.1.1 What is gravitational wave

In the General Theory of Relativity proposed by Albert Einstein in 1915, phenomena caused by gravity can be interpreted as results of curved spacetime. This is one of his important works after his 'Happiest Thought', which recorded in his unpublished article "Fundamental Ideas and Methods of the Theory of Relativity, Presented in Their Development"[2]. Among different ways to curve our spacetime, which can be described by corresponding metric tensor fields, there exist wavelike solutions describing ripples of spacetime known as gravitational waves.

However, the physical reality of gravitational wave was not so clear to everyone in the early days, even to Einstein himself [3, 4]. The main problem is that there exist some gauge degree of freedom in the theory due to the arbitrariness of coordinate choices. We have to know whether the gravitational waves we found are just gauge waves (vibration of coordinate) or the wave can have some observable consequences.

One of the most important observational evidence implying the existence of real gravitational waves is the Hulse-Taylor pulsar [5]. Taylor demonstrated that the change of pulsar rotation speed can be explained by emission of gravitational wave [6, 7].

Finally, on September 14th, 2015, the first direct detection of gravitational wave signal [8] is done by Laser Interferometer Gravitational-Wave Observatory(LIGO) detectors in the United States.

1.1.2 How to describe gravitational wave

In Einstein's General Relativity, gravitational effects are realized by geometry of spacetime. According to a great mathematician Bernhard Riemann, we can describe the geometry of certain space by telling the "distance" between nearby points in the space. Practically, the information of distance between nearby spacetime points form a tensor called metric, which means the measure of distance. By choosing a coordinate system, one can write down those corresponding components of metric tensor g.

$$g_{\mu\nu} = \begin{pmatrix} g_{00} & g_{01} & g_{02} & g_{03} \\ g_{10} & g_{11} & g_{12} & g_{13} \\ g_{20} & g_{21} & g_{22} & g_{23} \\ g_{30} & g_{31} & g_{32} & g_{33} \end{pmatrix} \tag{1.1}$$

Now, we can calculate spacetime distance ds between two nearby points by their coordinate separation:

$$ds^2 = g_{\mu\nu} dx^\mu dx^\nu \tag{1.2}$$

Through the interaction between matter and spacetime, matter can curve our Universe. The whole story can be resolved by solving Einstein equation,

$$R_{\mu\nu} - \frac{1}{2} g_{\mu\nu} R = \frac{8\pi G}{c^4} T_{\mu\nu} \tag{1.3}$$

which is a non-linear differential equation of metric tensor field $g_{\mu\nu}(x^\alpha)$ since the Ricci tensor $R_{\mu\nu}$ contains metric tensor and its differential.

It's similar to the case in Electrodynamics, in which we can have electromagnetic waves solutions by solving Maxwell equations in vacuum, that we can have gravitation

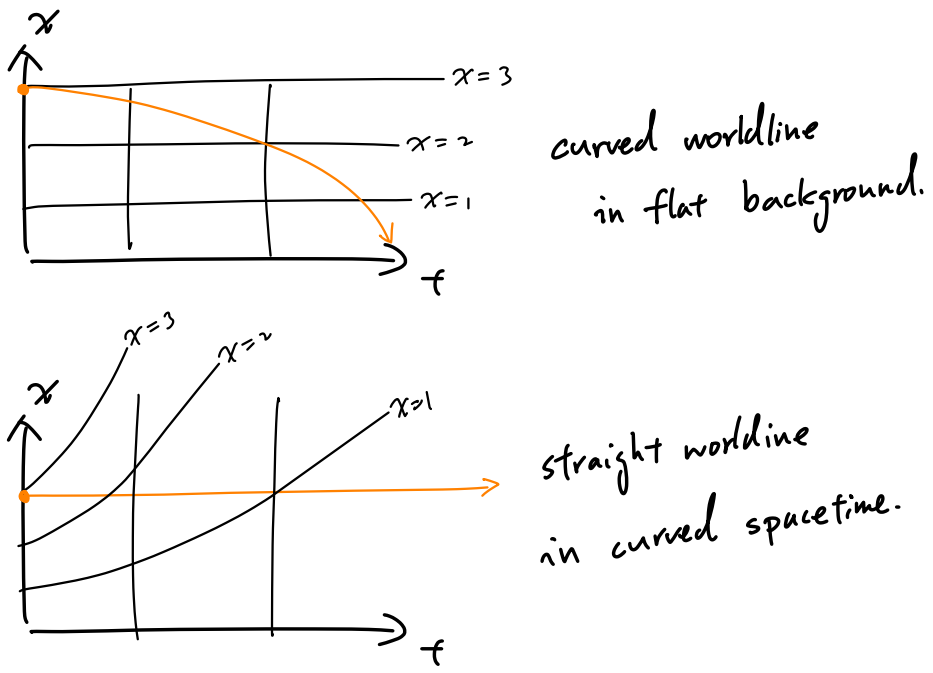

Figure 1.1: Newtonian versus Einstein's point of view.

wave solutions by solving vacuum Einstein equation. The situation will become even clear if we linearize the Einstein equation and choose coordinate or gauge properly.

A wave equation derived from linearized Einstein equation can be expressed in following way

$$\Box \bar{h}_{\mu\nu} = -\frac{16\pi G}{c^4} T_{\mu\nu} \tag{1.4}$$

Where $\bar{h}_{\mu\nu}$ is the trace-reversed metric perturbation on flat spacetime background.

the corresponding coordinates are attached to a set of free falling objects. for perturbation of wave like part metic over Schwarzschild background which represent Earths gravity. Refer to [9]

1.1.3 How to generate gravitational wave

The source of electromagnetic wave is time-dependent electrical charge distribution. Similarly, the source of gravitational wave is time-dependent mass(energy) distribution. Strictly speaking, the lowest order of mass multi-pole which can generate

real gravitational waves in GR is mass quadruple, while the electromagnet wave can be generate though time-dependent electrical dipole moment. The gravitational wave strain generated by mass quadruple can be approximately described by famous quadrupole formula: (quadrupole formula) Practically, PN NR.... According to our current understand of universe, there are several kinds of astrophysical gravitational wave sources, whose h(t) amplitude is large enough to be detected by current ground based laser interferometer, like advanced-LIGO, advanced-Virgo or KAGRA. Compact Binary Coalescence BNS BBH

1.1.4 How to detect Gravitational wave

The interaction of detector and gravitational wave can have different interpretation due to different coordinate choice[10]. It is quite similar to that the magnetic force in one observational frame may be electric force in the other frame. However, practically, I would like to use the .., which described in next section.

1.2 Detection of Gravitation wave

Interaction of GW wave when $\lambda_g w$ L of detector Limit of Michelson IFO IFO with dual-recycling and Fabry-Perot arms. Complex response WE NEED Calibration Calibration Calibration

1.3 Calibration and Reconstruction

Calibration is always the fist step before we measure something by some device. For example, to measure the weight of an apple, you should calibrate your scale by putting a standard kilogram on it. Then, you can either adjust the scale readout to be 1kg, or record the difference showed in scale readout, which may be used to reconstruct real

weight of the apple. However, the spring constant of springs inside the scale could fluctuate due to temperature changes. To accurately measure the weight of the apple, we have to measure the calibration factor (scale readout when we put the standard mass on it.) when we measure the weight of apple, if possible, simultaneously.

Due to the complexity of practical interferometer, the response of interferometer itself to external gravitational source is not only sophisticated but also time-dependent. In reality, we inject several calibration lines, which means we displace the End-Test-Mirror by several known frequency and amplitude sine waves. Then, we try to see these standard signals in the readout of interferometer, thereby solving the response of interferometer.

1.3.1 Transfer function of Laser Interferometer with Fabry-Perot Cavity

1.3.2 Tracking Time-dependent Response by Calibration lines

1.4 Photon Calibrator (Pcal)

1.4.1 Principle of Photon Calibrator

Photon calibrator is an additional laser with high precision intensity modulator. It is installed in front of End-Test-Mass Mirror(ETM) and can push the ETM by radiation force due to its own Laser beam as depicted in Fig.(1.2). To generate any artificial h(t) by Pcal, we have to translate desired h(t) into corresponding force F(t) exerting on ETM. This can be done by using equation of motion of the ETM suspend by its suspension system. Then, we control the Pcal Laser output intensity P(t) such that the radiation force exerted on ETM is F(t) we calculated before.

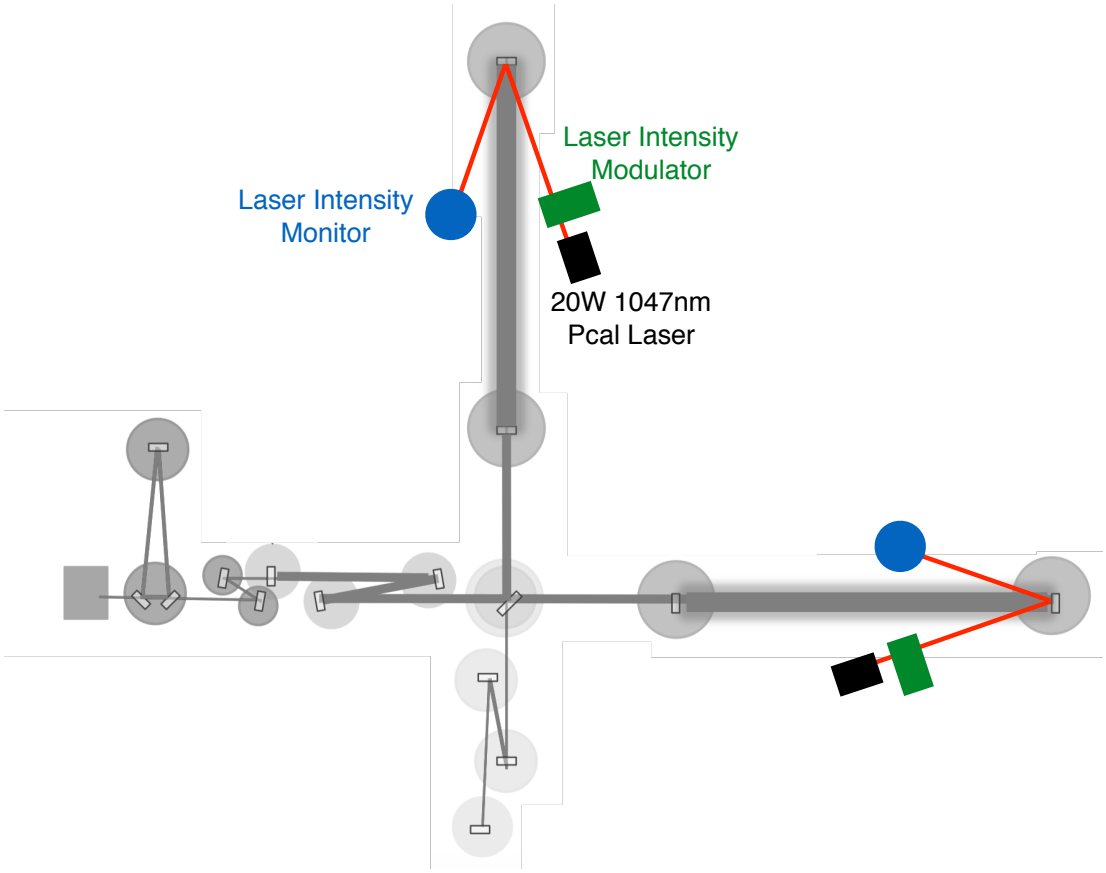

Figure 1.2: Schematic Diagram of KAGRA Photon Calibrator. Two sets of Photon Calibrators have been installed in front of ETMX (X-arm End-Tess-Mirror) and ETMY

The radiation force caused by a continuous laser beam can be calculated by its momentum transfer per unit time.

$$\mathbf{F} = \frac{\Delta \mathbf{p}}{\Delta t} \tag{1.5}$$

For our purpose, the laser beam will be almost reflected from ETM. Therefore, the momentum transfer to ETM per unit time should be almost equal to twice of longitudinal momentum flux carried by PCal laser beam.

$$\mathbf{F}_{\text{on ETM}} = \frac{\Delta \mathbf{p}_{\text{ETM}}}{\Delta t} = 2\cos(\theta)\frac{\Delta p_{\text{Laser}}}{\Delta t} \tag{1.6}$$

where θ is the angle of incident.

Furthermore, one can express the momentum flux of light in terms of its intensity through Eq.(1.10), which can be derived from either classical point of view with its Poynting vector or Quantum Mechanical approaches that we adopt here by dealing with photons.

$$E_\gamma = \hbar\omega \tag{1.7}$$

$$p_\gamma = \hbar k \tag{1.8}$$

$$= \frac{k}{\omega}\, E_\gamma = \frac{1}{c} E_\gamma \tag{1.9}$$

$$\underbrace{\frac{\Delta p_{\text{photons}}}{\Delta t}}_{\substack{\text{momentum flux due to} \\ \text{photons in a continuous laser beam}}} = \frac{1}{c} \underbrace{\frac{\Delta E_{\text{photons}}}{\Delta t}}_{\substack{\text{Intensity of laser beam} \\ \text{defined as } P}} = \frac{P}{c} \tag{1.10}$$

Combining Eq.(1.6) and Eq.(1.10), the force that PCcal can give ETM is:

$$F_{\text{PCal}}(t) = \frac{2\cos(\theta)}{c} P(t) \tag{1.11}$$

On the other hand, the equation of motion of suspend ETM with mass M can be modeled as:

$$\ddot{x}(t) + b\dot{x}(t) + \omega_0^2 x(t) = \frac{F(t)}{M} \tag{1.12}$$

where $M\omega_0^2 x(t)$ is the restoring force from suspension system and $Mb\dot{x}(t)$ is the damping force. Both of them are calculated up to leading order since the displacement amplitude and the velocity of ETM are suppose to be small.

The impulse response of Eq.(1.12) is

$$x(t) = \frac{b}{\omega_1} e^{-\frac{b}{2}(t-t_0)} \sin[\omega_1(t-t_0)] \tag{1.13}$$

where $\omega_1 = OO$ is the resonance frequency of damped oscillator.

And in frequency domain, we have

$$x(\omega) = \frac{-1}{\omega^2 - \omega_0^2 - i\omega b} \frac{F(\omega)}{M} \tag{1.14}$$

As long as $\omega^2 \gg \omega_0^2$ and $\omega \gg b$, Eq.(1.14) can be approximated as

$$x(\omega) = \frac{-1}{\omega^2} F(\omega) \tag{1.15}$$

By substituting the Fourier transformed Eq.(1.11) into Eq.(1.15), we can get the expression of $x(\omega)$ by frequency domain PCal laser intensity modulation $P(\omega)$

$$x(\omega) = \frac{-1}{M\omega^2} \frac{2P(\omega)\cos(\theta)}{c} \tag{1.16}$$

1.4.2 Evolution of Photon Calibrator

The original PCal was proposed by Glasgow group [11] in order to calibrate their 10 meter interferometer prototype. With the PCal, they can displace the mirror of their arm cavity without attaching extra components, e.g. magnets, on the mirror, that might change its mechanical properties like Q-factor resulting unwanted side-effect.

In their experiment, they used a single laser beam hitting on the center of ETM and successfully see these sin waves in the the readout of their interferometer. Later on, GEO.

is that it may introduce drumhead mode vibration of ETM surface (just like the vibration mode you see when you hit the center of a drum), which introduce unwanted h(t) effectively. This problem is solved by LIGO group[12], who separate the Pcal laser beam into two beams, hitting on the nodal point of drumhead mode on the

ETM surface[13]. In order to excite same amplitude h(t) in higher frequency regime, we have to give much larger F(t) since the relationship between x(t) and F(t) in an pendulum .

1.4.3 Why do we need Photon Calibrator

1.4.4 Tracking Time-dependent Response by Calibration lines

Chapter 2

Hardware Injection through Photon Calibrator

2.1 Principle

As I described in Sec.1.4.1, we can generate desired ETM displacement $x(t)$ by changing PCal laser intensity $P(t)$. One can calculate corresponding $P(t)$ by performing inverse Fourier transform to Eq.(1.16).

$$\int_{-\infty}^{-\infty} x(\omega) e^{i\omega t} \, \mathrm{d}\omega = \frac{-2\cos(\theta)}{Mc} \int_{-\infty}^{-\infty} \frac{P(\omega)}{\omega^2} e^{i\omega t} \, \mathrm{d}\omega \tag{2.1}$$

$$\frac{Mc}{-2\cos(\theta)} \int_{-\infty}^{-\infty} x(\omega)\omega^2 e^{i\omega t} \, \mathrm{d}\omega = P(t) \tag{2.2}$$

where

Mass of ETM	$M = 23$ kg
Arm Length	$L = 3$ km
Angle of Incident	$\theta = 0.72$ deg
Speed of Light	$c = 2.998 \times 10^8$ m/s

Also, if we have complete suspension model of ETM, we can substitute the ω^2 factor in Eq.(2.2) by the full displacement-to-force transfer function.

2.2 Experimental Setup

Once we got the necessary P(t) from the desired x(t) through Eq.(2.2), we can start to modulate our PCal laser intensity according to that P(t). The way how we control our PCal laser intensity is explained in Fig. (2.1).

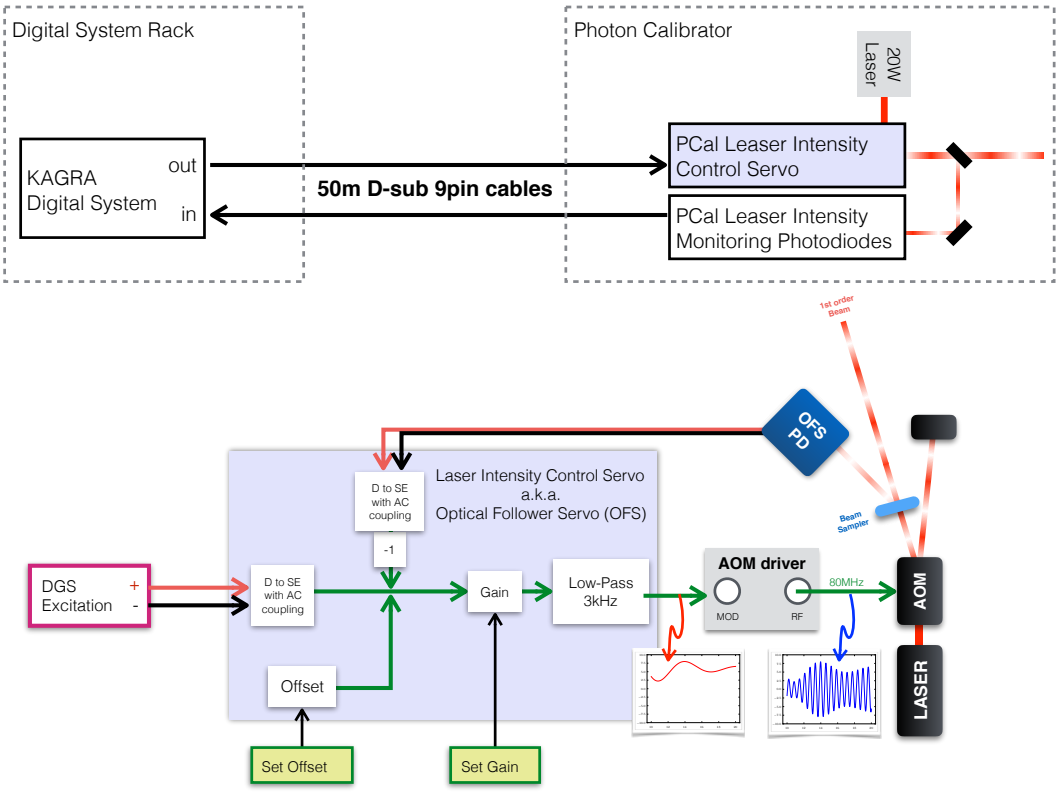

Figure 2.1: Controlling PCal with Digital Control System. The PCal laser beam that will be sent to ETM is the first order diffracted beam of a 20W input laser form an acousto-optic modulator(AOM). Its intensity is controlled by the control signal from our KAGRA Digital System. An analog feedback control loop called Optical Follower Servo(OFS) has been implemented to reduce non-linear response of AOM and laser intensity noise of 20W input laser.

Chapter 3

Signal Generating System

3.1 KAGRA Digital Control System

The Digital Control System used in KAGRA is based on the Advanced LIGO Digital System [14]. In this system, analog control signals can be generated from a Digital-to-Analog Convertor(DAC) installed in any realtime computer known as a Front-End machine located around interferometer. Between the DAC output and experimental device, a customized analog low-pass filter called an Anti-Image filter [15] has been installed for removing unwanted high frequency signal, the Image, due to digitized output from DAC.

Inside a Front-End machine, the signal that will be sent to a DAC are prepared by a realtime software [16], which is generated from several building blocks, realtime models, by a customized parser and compiler [17]. Each realtime model can be running at specifiable sample rate on a dedicated CPU core. However, currently, all DAC cards installed at KAGRA site are 16bit, 64kHz (65536Hz) ones. Therefore, a mandatary model named Input/Output Processor(IOP) model will always run at 64kHz [16], communicating with a DAC card and other "slave" models, in which people can put digital filters, signal generators, etc [18].

On the other hand, the digital system also works as a Data Acquisition System (DAQ). An analog signal coming from a transducer (e.g. a photodiode) can be sampled by an Analog-to-Digital Convertor(ADC). After that, processed by optional digital filters, it could be sent back to an experimental device trough a DAC, be analyzed by an online diagnosis tool, or be stored into a frame file through the frame-builder. To avoid aliasing effect, which is caused by a finite sampling rate, a customized analog low-pass filter, which has the same circuit design as the AI filter, called an Anti-Alias filter [15] has been inserted between the incoming signal and the ADC card. Reference!!! Reference!!!

Unfortunately, the noise performance of such general purpose system do not meet the requirement of KAGRA Photon Calibrator in current setup. The noise coming from the digital system output can be directly translated into the PCal laser intensity noise, which will displace the ETM in a noisy way.

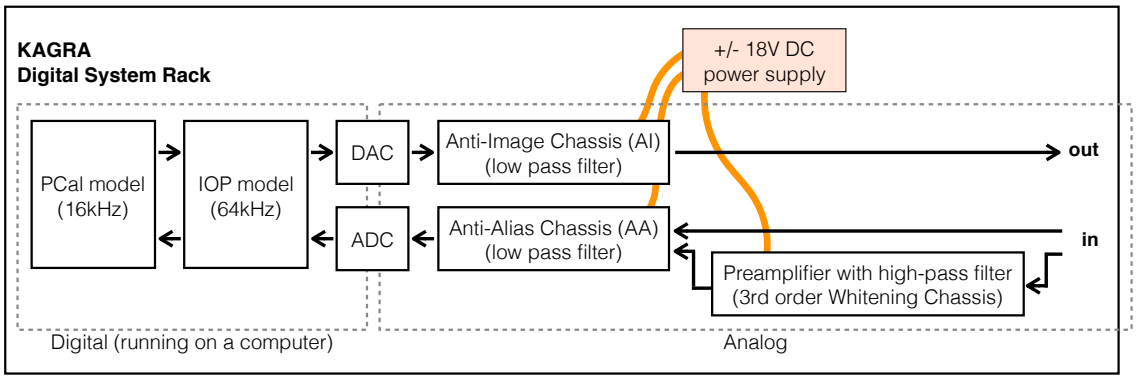

Figure 3.1: The schematic shows the inside of the KAGRA digital system block in Fig. (2.1). A optional whitening chassis is used as a preamplifier that only amplify the signal above 10Hz.

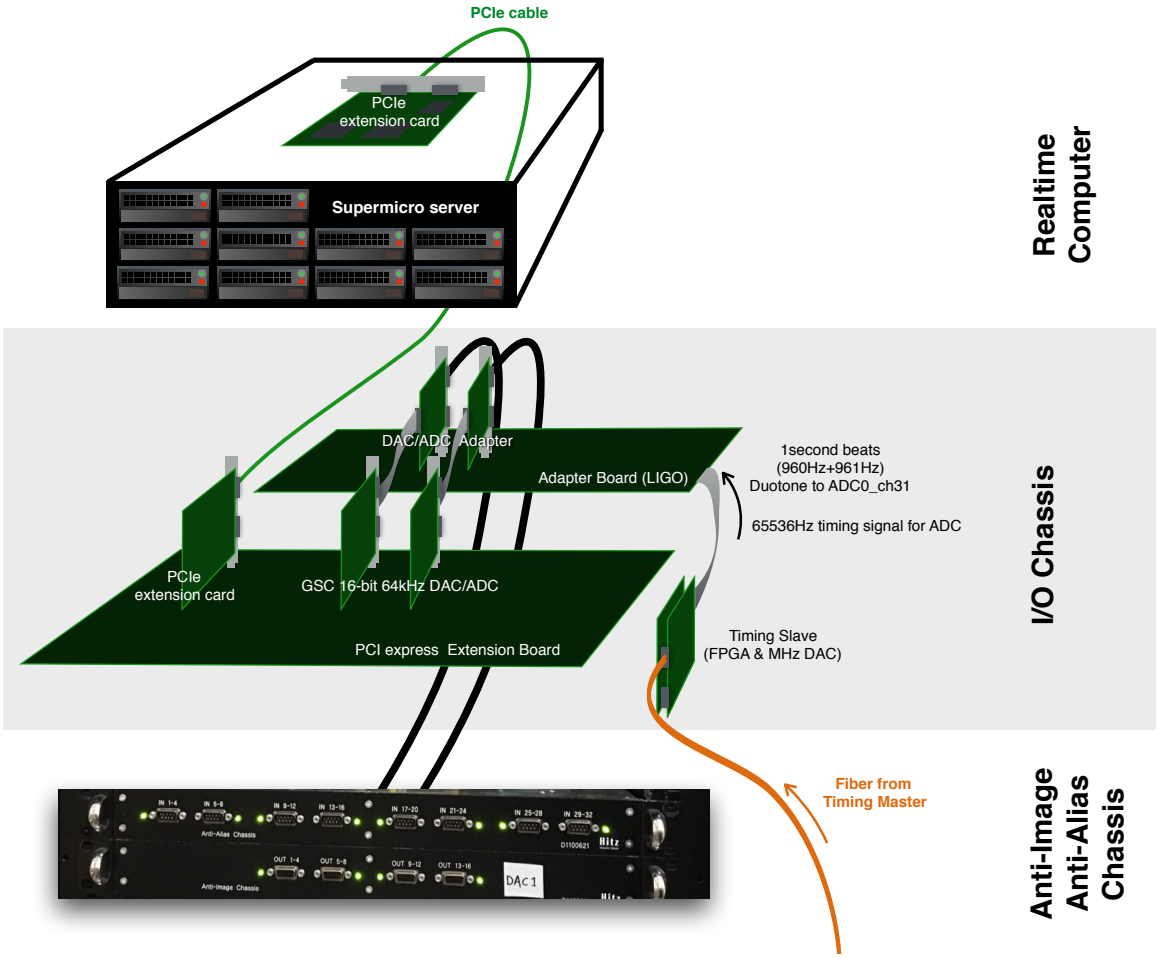

Figure 3.2: dgs

3.2 Noise Problem of Injection Signal

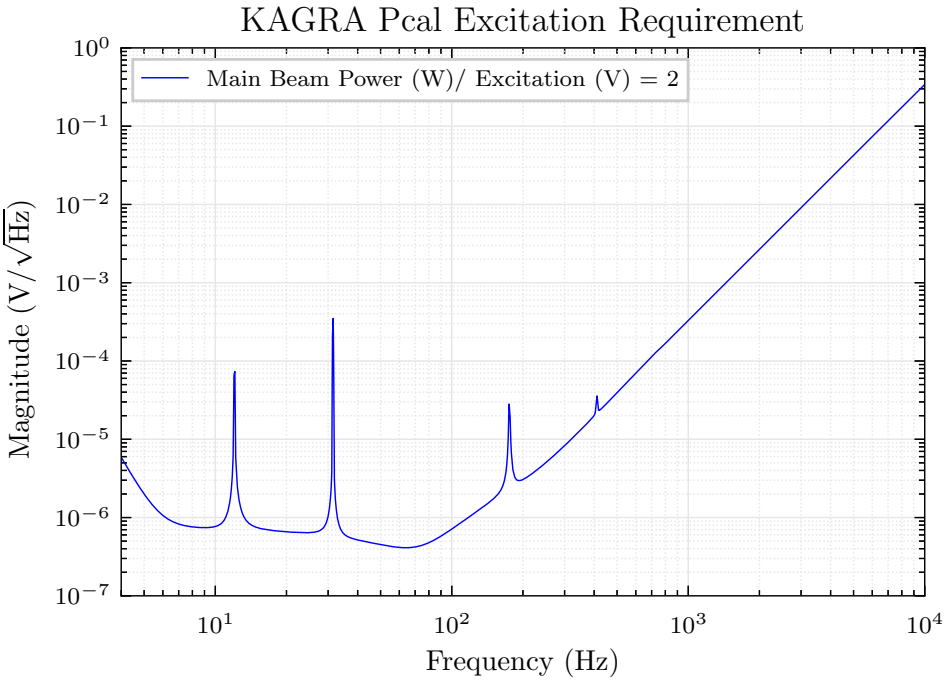

Figure 3.3: Injection Channel Noise Requirement

$$\Delta L(f) < \frac{1}{10} \times (\text{KAGRA length sensitivity}) \tag{3.1}$$

$$\Delta L(f) = \frac{2\Delta P(f)\cos(\theta)}{c} \frac{1}{M(2\pi f)^2} < \frac{1}{10}\Delta h(f) L \tag{3.2}$$

3.2.1 Noise Sources from Control Signal

Quantization Noise of DAC

The origin of quantization error is coming from the difference between desired analog output and quantized Digital to Analog Converter(DAC) output value. Roughly speaking, it shows up like white noise that is spread from DC to Nyquist frequency, i.e. $Fs/2$. The Root Mean Square value of quantization noise has the order of voltage difference corresponding to last digit or Least Significant Bit(LSB). In time domain,

we can calculate standard deviation.

$$\sigma_x = \sqrt{\frac{1}{12}}\delta x_{LSB} \tag{3.3}$$

For a 16-bit 64kHz DAC with output range between ±10Volts,

$$\sigma_x = \sqrt{\frac{1}{12}}\delta x_{LSB} \tag{3.4}$$

$$= \sqrt{\frac{1}{12}}\frac{(+10) - (-10)\text{Volts}}{2^{16}} \tag{3.5}$$

$$= 8.81 \times 10^{-5} \text{ Volts} \tag{3.6}$$

In frequency Domain, the quantization noise is distributed from DC to 32768Hz; therefore, we have ASD

$$ASD = \sqrt{PSD} \tag{3.7}$$

$$= \sqrt{\frac{\sigma_x^2}{32768}} \tag{3.8}$$

$$= 8.81 \times 10^{-5}\sqrt{\frac{1}{32768}} \tag{3.9}$$

$$= 4.87 \times 10^{-7} \text{ Volts}/\sqrt{\text{Hz}} \tag{3.10}$$

Analog circuits

AC Power Line

Chapter 4

Noise Reduction through De-Whitening Filter

4.1 Concept of De-Whitening Filter

Considering a situation in which the Photon Calibrator received white, i.e. frequency independent, excitation signal noise, it will generate $1/f^2$ displacement noise on End-Test-Mirror because the force to displacement transfer function contains $1/f^2$ feature. If we put an analog filter that has frequency response proportional to f^2 between excitation signal and PCal excitation input port, we may create colored, f^2, laser intensity noise from white electrical noise of excitation signal. Then, such colored noise will be whitened by $1/f^2$ force to displacement transfer function, becoming white displacement noise. We call the f^2 analog filter *De-Whitening filter*.

Practically, we use a one pole one zero analog filter with transfer function showed in Fig.(4.1) as our De-Whitening filter.

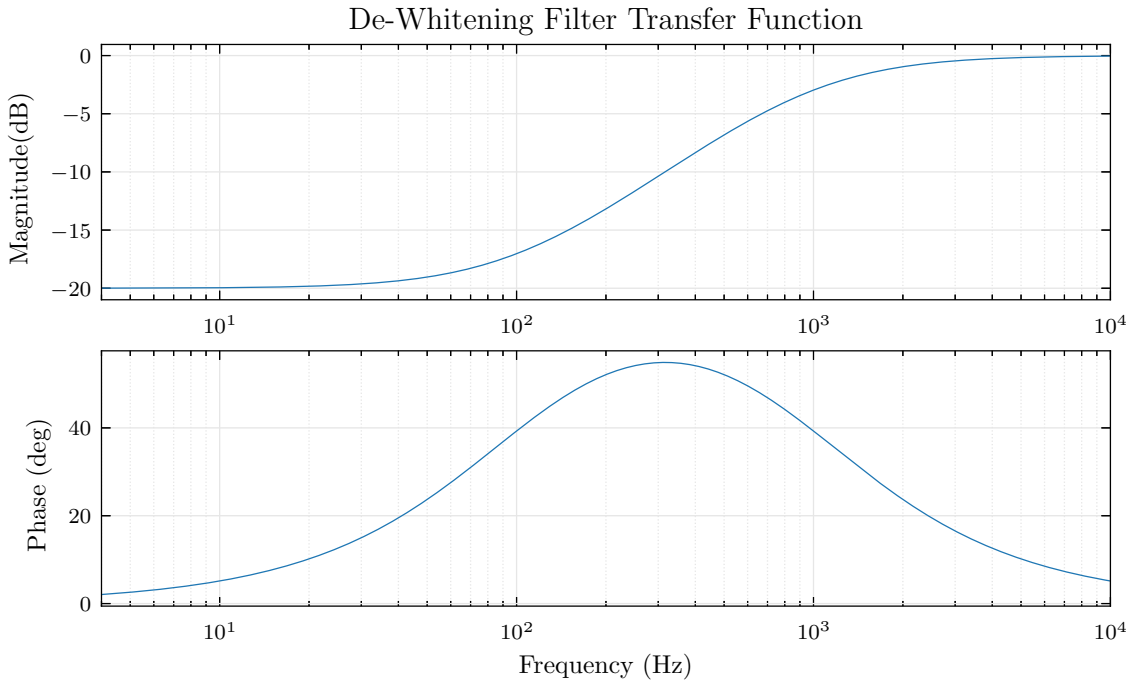

Figure 4.1: De-Whitening filter transfer function. This is the deigned transfer function of De-Whitening filter. It has a pole at 1kHz and a zero at 100Hz.

4.2 Circuit Design

The main circuit design is described in Fig. 4.2. It converts a differential input signal into a single-ended one by an instrumentation amplifier. Then, the signal will pass through the De-Whitening stage, which attenuates the low-frequency signal while keeping the gain of the high-frequency signal unchanged. After that, we convert the filtered single-ended output to differential output, and send it to a downstream device.

The frequency dependent attenuation in the De-Whitening stage is realized by a single zero-pole analog filter. The pole and zero frequencies are determined by resistors and capacitors between A and B in Fig. 4.2. In order to reduce filter shape uncertainty caused by pole-zero frequency drifting, we use 0.01μF Mica capacitor (CD30FD103FO3F made by Cornell Dubilier Electronics), whose capacitance tolerance is within 1% and capacitance drift is within $\pm(0.05\% + 0.1pF)$.

The transfer function of this circuit is

$$\text{DewTF} = \underbrace{\frac{Z_A}{Z_A + Z_B}}_{\text{pole-zero stage}} \times \underbrace{2}_{\text{Single to Differential}} \tag{4.1}$$

where

$$A//B \equiv \frac{1}{\frac{1}{A} + \frac{1}{B}} \tag{4.2}$$

$$Z_B = (R_3 + \frac{1}{i\omega C_2}) \;//\; R_b \tag{4.3}$$

$$Z_A = (R_4 + \frac{1}{i\omega C_1}) \;//\; R_a \tag{4.4}$$

When $R_3 = R_4 = a$, $C1 = C2 = C$, Eq. (4.1) will reduce to

$$\text{DewTF} = 2\left(\frac{1 + i\omega C(a + R_b)}{1 + \frac{R_b}{R_a} + i\omega C(2R_b + a(1 + \frac{R_b}{R_a}))}\right) \tag{4.5}$$

Practically, we chose $a = 100\Omega << R_a = 8.34(88)\text{k}\Omega < R_b = 159.(3)\text{k}\Omega$. Then, the DC gain is

$$\text{DewTF} \;|_{\omega=0} = \frac{2}{1 + \frac{R_b}{R_a}} = 0.0996 \tag{4.6}$$

It is about a factor of ten suppression of low-frequency signals while gains of high-frequency signals are kept unity. The pole and zero frequencies of such circuit are

$$\text{Zero} = \frac{1}{2\pi C(a + R_a)} = OOO\text{Hz} \tag{4.7}$$

$$\text{Pole} = \frac{1}{2\pi C(a + 2\frac{R_a R_b}{R_a + R_b})} = OOO\text{Hz} \tag{4.8}$$

An overall transfer function simulated with LTspice is shown in Fig. XX

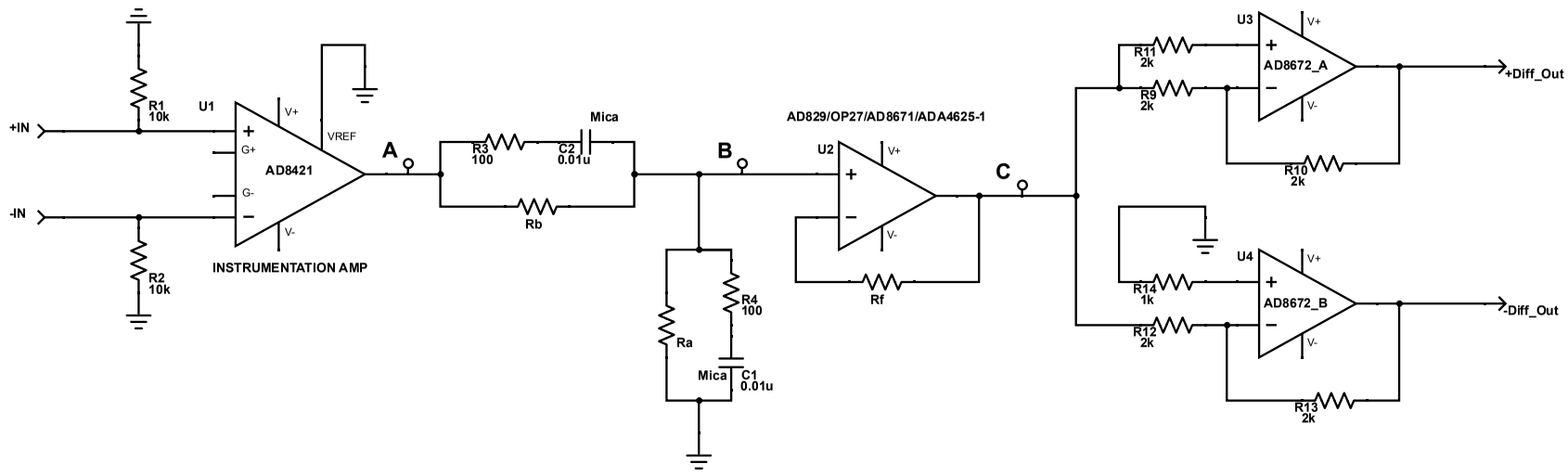

Figure 4.2: De-Whitening filter circuit. There are three points labeled as A, B, and C in the diagram. Before A, a differential input signal provided by Digital System will be converted into a single-ended signal by an instrumentation amplifier AD8421. After that, a passive pole-zero stage between A and B defines the dominate transfer function of the De-Whitening filter. Then we put a voltage follower between B and C as a buffer to keep passive filter response. Finally, we convert the signal back to a differential output to match the downstream device input.

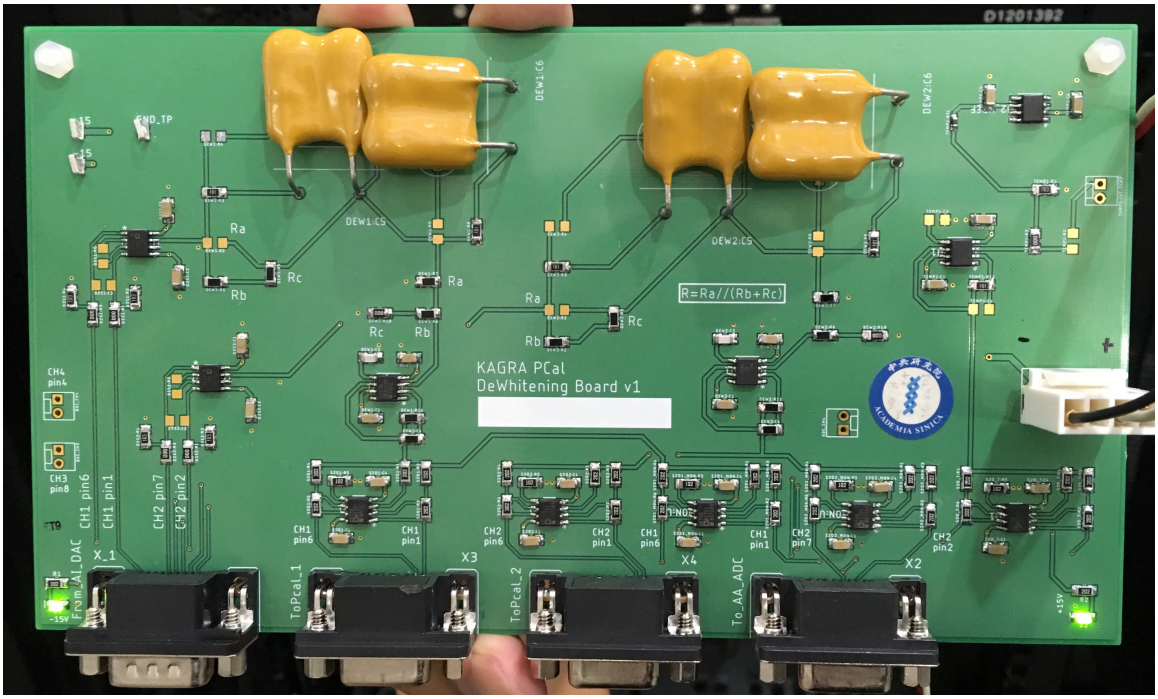

Figure 4.3: De-Whitening filter board. It's a 1.6mm FR-4 printed circuit board manufactured by SPEEDY Circuits Co., Ltd. The layout of this board is done with EAGLE, an EDA software. Four large yellow capacitors are Mica capacitors for the pole-zero stage. At KAGRA site, we installed it into a 1U chassis powered by a DC power supply with LM317/LM337 voltage regulation circuit designed by LIGO.

4.3 Fidelity of Injection Signals

The fidelity of injected signals is the fundamental requirement of hardware injection test. One can estimate the distortion of the injected waveforms by measuring the transfer function between an excitation port in the software and the PCal laser intensity. After measuring such transfer function, we can create an inverse De-Whitening digital filter in software side to compensate for our analog De-Whitening filter. The combination allows as to suppress low-frequency noise from DAC while the transfer function for signal is kept unity.

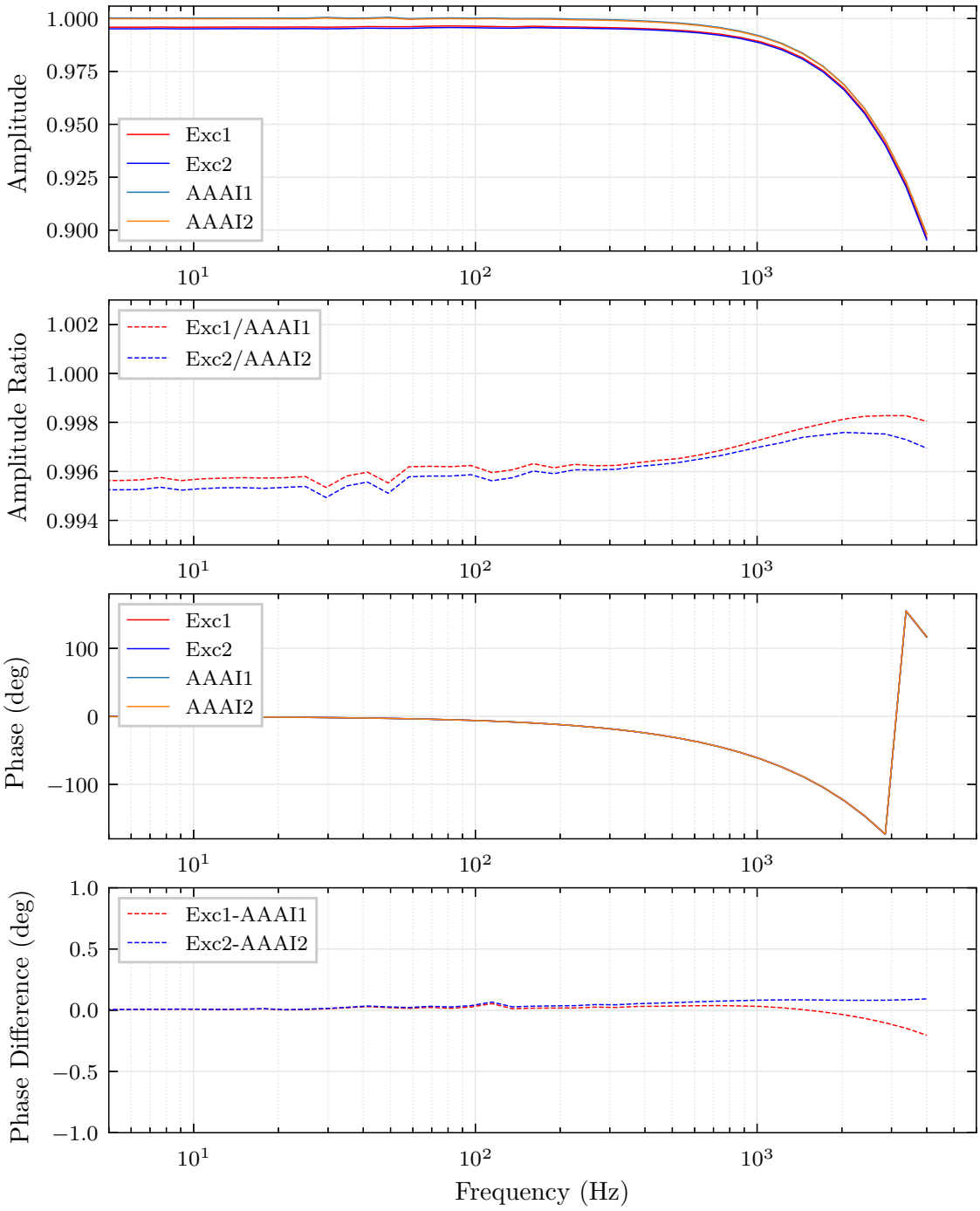

Figure 4.4: Transfer function of De-Whitening Filter with Digital Inverse Filter. The transfer function is measured in KEK cryogenic center with KAGRA standalone digital system and 64kHz salve model.

4.4 Noise Reduction Performance

We have tested the noise reduction performance of our De-Whitening Filter in KAGRA X-END. The noise is measured by the KAGRA Digital System with a third order whitening filter, which can amplify the signal above 10Hz for about 60dB. Exactly speaking, it has a third order zero at 10Hz and a third order pole at 1Hz in its amplification circuit.

The experimental setup is depicted in Fig. 4.5 and Fig. 4.6.

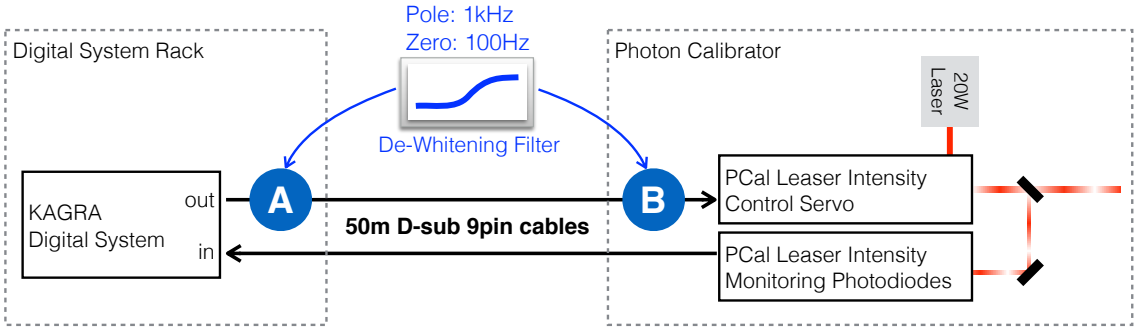

Figure 4.5: In order to reduce the noise coming from the digital system, the De-Whitening filter can be installed at either place A or B.

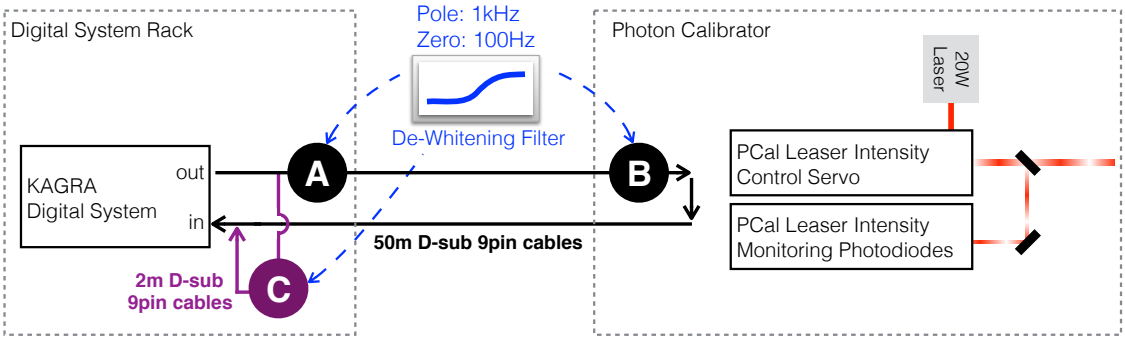

Figure 4.6: For our reference, we also measured the noise from the digital system without passing through the control loop of PCal. Place C means we connect De-Whitening filter in digital system rack with 2m cable only in order to investigate the influence from 50m cable.

The acronym used in legends in measurement plots are explained in Table 4.1.

Label in legend	Description
AI	Anti-Alias Chassis with Whitening Filter (as a preamplifier)
AA	Anti-Image Chassis
DEW	De-Whitening Filter

Table 4.1: Acronym of devices in noise measurement plots

4.4.1 Noise Measurement without PCal System

As described in Fig.(4.6), we have compared the noise from digital control system through different cable length with and without De-Whitening filter.

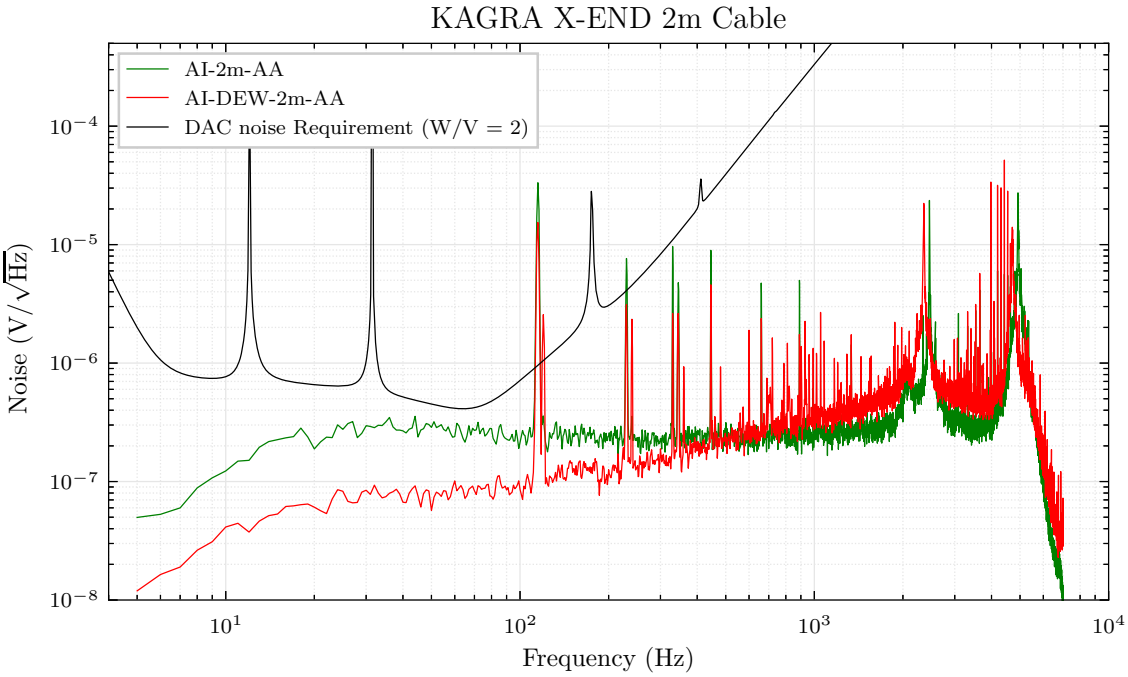

Figure 4.7: De-Whitening filter noise with short (2m) cable. The green line is the noise without De-Whitening filter, while the red one is the noise with De-Whitening filter.

Fig.(4.7) is the noise measurement result with 2m signal cable as described in Fig.(4.6). The low-frequency noise is suppressed by De-Whitening circuit. However, the amount of suppressing is not 20dB. It is possible that we hit another noise floor at $10^{-7}\mathrm{V}/\sqrt{\mathrm{Hz}}$ due to the internal noise of the De-Whitening filter circuit. Below 10Hz, the measured noise is less than actual noise since we used the a customized high-pass filter, i.e. a Whitening Chassis, to prevent the saturation of measurement instrument by any small DC offset. Same effect is exist in all noise measurement results in this thesis since we adopted same measuring scheme.

In the end station of KAGRA, unfortunately, the digital system rack is placed near the ETM, which is 36m far away from PCal system. Therefore, the practical control

signal is carried by 50m D-sub cables as illustrated in Fig.(4.5) at this moment. As a result, we tried to perform the same noise measurement with 50m cables. The result is in Fig.(4.8).

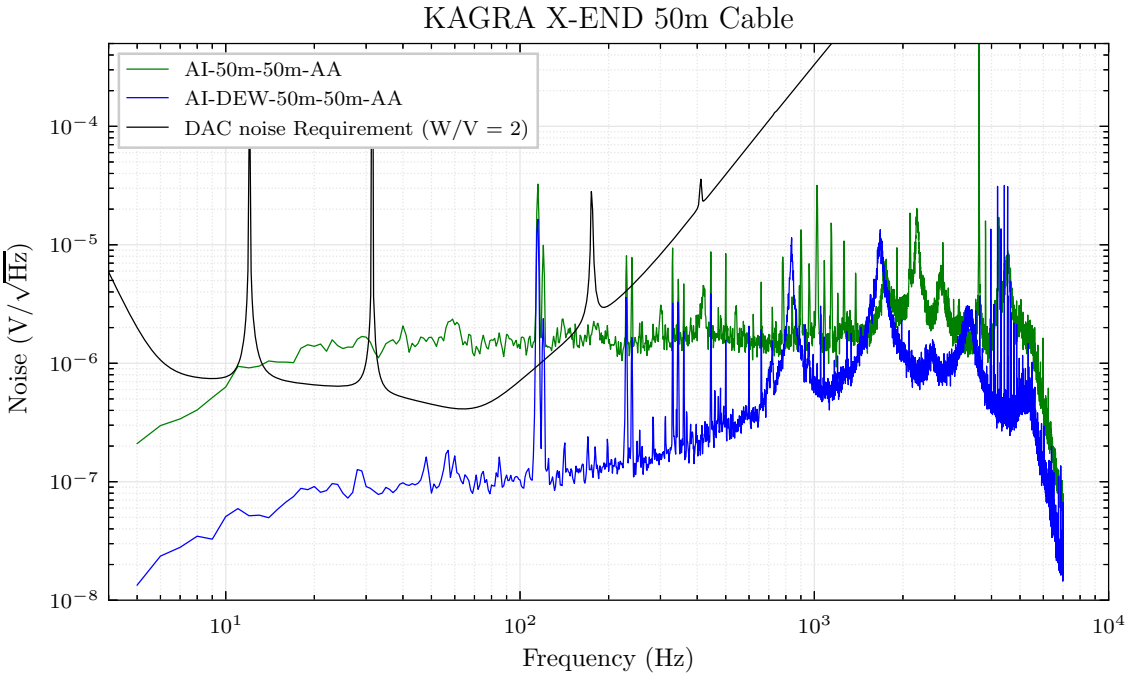

Figure 4.8: De-Whitening filter noise with long (50m) cable.

With 50m cable, the unsuppressed noise (green line in Fig.(4.8)) is larger than 2m one (green line in Fig.(4.7)) due to unknown reason. However, the 20dB suppression capability can be verified in Fig.(4.8).

In Fig.(4.9), we overplot the suppressed noise by De-Whitening filter in 2m and 50m cable case. Although the 50m case has some noise excess around kHz regime, their low-frequency noise performance do not have significant difference. This result imply that the $10^{-7}\mathrm{V}/\sqrt{\mathrm{Hz}}$ noise floor can really come from De-Whitening circuit itself. In the future, we may come back into this issue when we have more strict noise requirement that will be the case if we decide to use higher power Pcal laser or have better interferometer sensitivity.

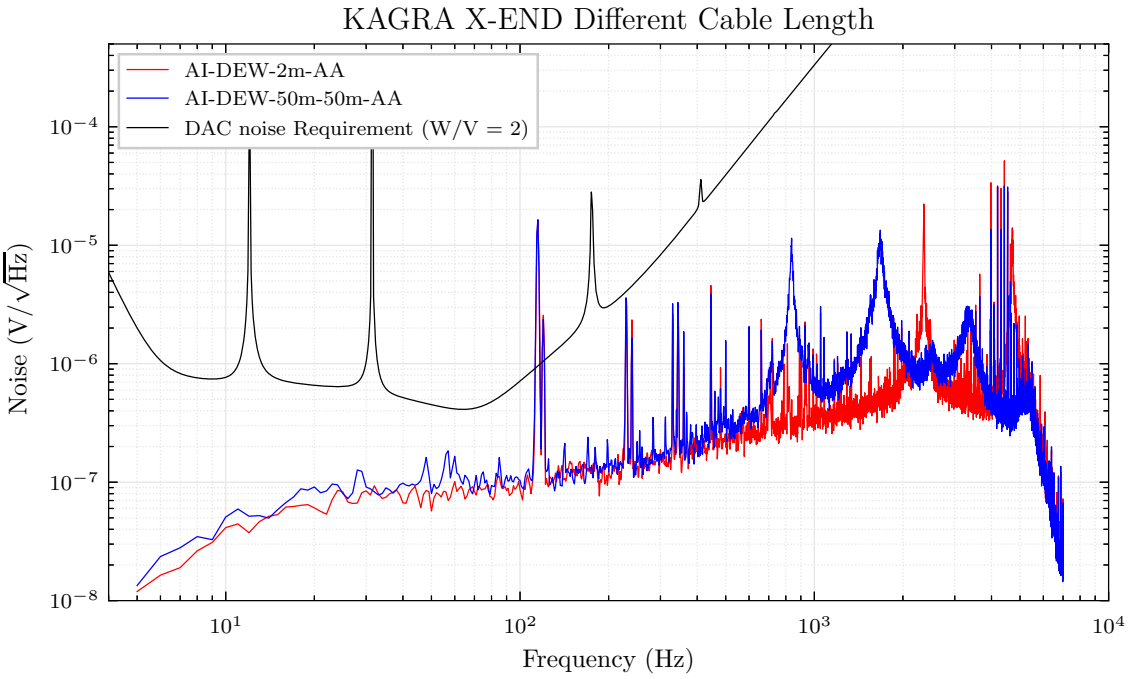

Figure 4.9: De-Whitening filter noise with different cable length.

Since we observed that the unattenuated noise floor in 50m cable case is larger, we suspect that some environmental noises are picked up by the cable. We tried to install our De-Whitening filter in either place A or B in Fig.4.6 and the result is in Fig.4.10. Originally, we thought if the extra noise is picked up by the cable, it should be attenuated when we install the De-Whitening filter at place B. However, the red line in Fig.4.10 shows that if we put our De-Whitening filter at place B, the measured noise is actually higher than the one without De-Whitening filter.

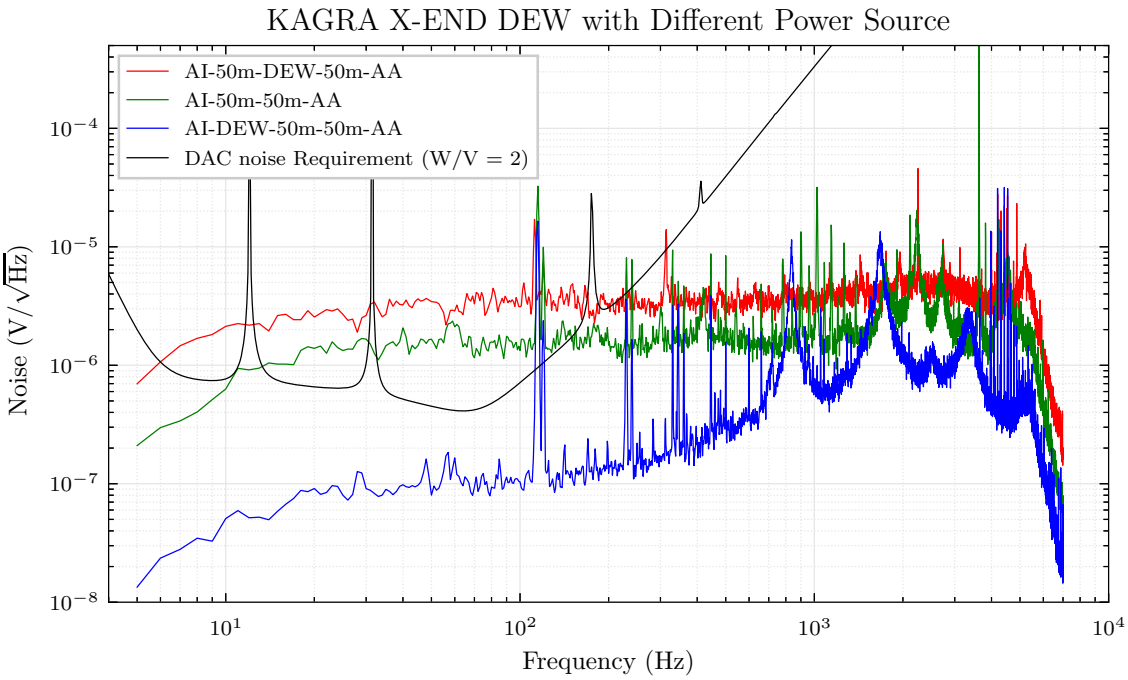

Figure 4.10: Noise measurement when the De-Whitening filter is installed at different location.

4.4.2 Noise Measurement with PCal System

Now, it is the time to connect the Digital System and the De-Whitening filter to our Photon Calibrator. The practical setup is illustrated in Fig. 4.5.

First, we try to understand how much low-frequency noise could be suppressed by De-Whitening filter. However, Fig. 4.11 indicates that something bad happened. Even though in the case with the De-Whitening, the noise decreases from blue line to red line in Fig. 4.11, it dose not follow the transfer function of De-Whitening filter, which can only suppress low-frequency noise.

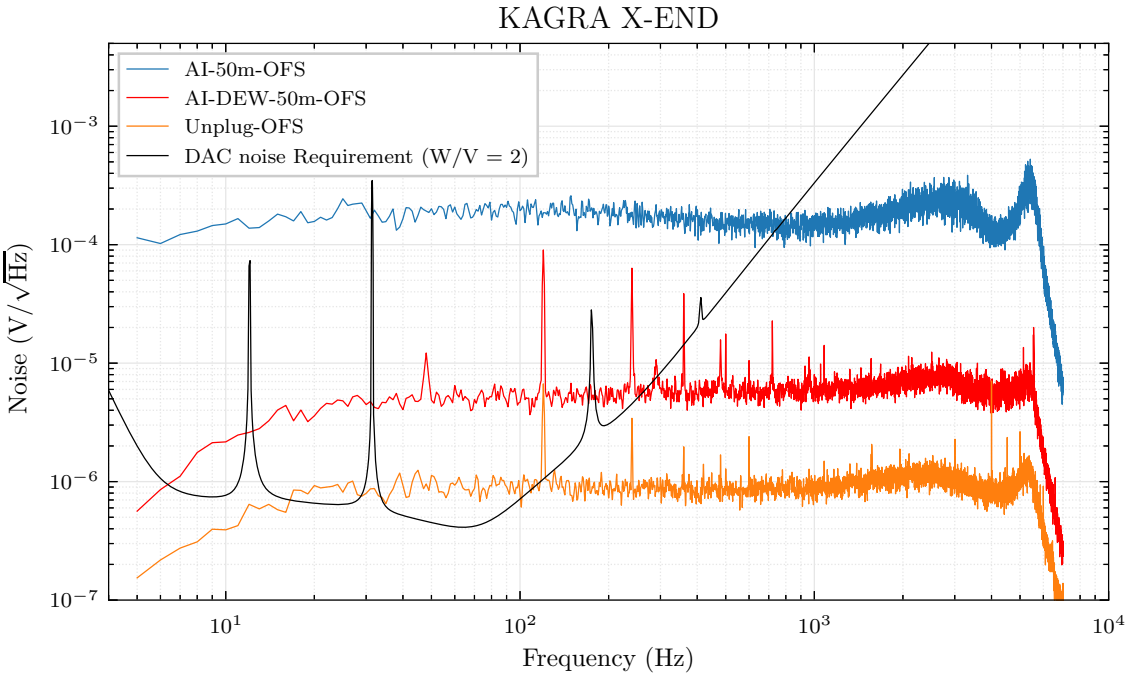

Figure 4.11: Noise measurement with PCal. These noises can be considered as laser intensity noises since we are measuring photodiode readout as depicted in Fig. 4.5. The blue line is the case without De-Whitening filer, while the red line is the case when De-Whitening filer has been installed at place A in Fig. 4.5. The orange line is measured when we disconnect our signal cable from the Laser Intensity Control Servo input port.

On the other hand, the orange line is the nosies when we disconnect the digital system output from our PCal. It is lower than either one of connected cases (blue and red). Besides, it is also higher than the noise that are plotted in Fig.(4.9), which is supposed to be the noise that be sent to PCal from the output of De-Whitening

filter. It reveals that the blue and the red lines in Fig. 4.11 is actually popped out just when we connect the digital system and our PCal together. We doubt that we may create the infamous grounding loop unintentionally. As a trial, we tried two different measurements. First, we put our De-Whitening filter in either palace A or B in Fig. 4.5 and the result is in Fig. 4.12. Second, we supplied our Pcal from the DC power source located at digital system rack, which is shared with De-Whitening filter and other analog chassis of the digital system, including Anti-Image, Anti-Alias, and Whiting chassis. The result is given in Fig. 4.13.

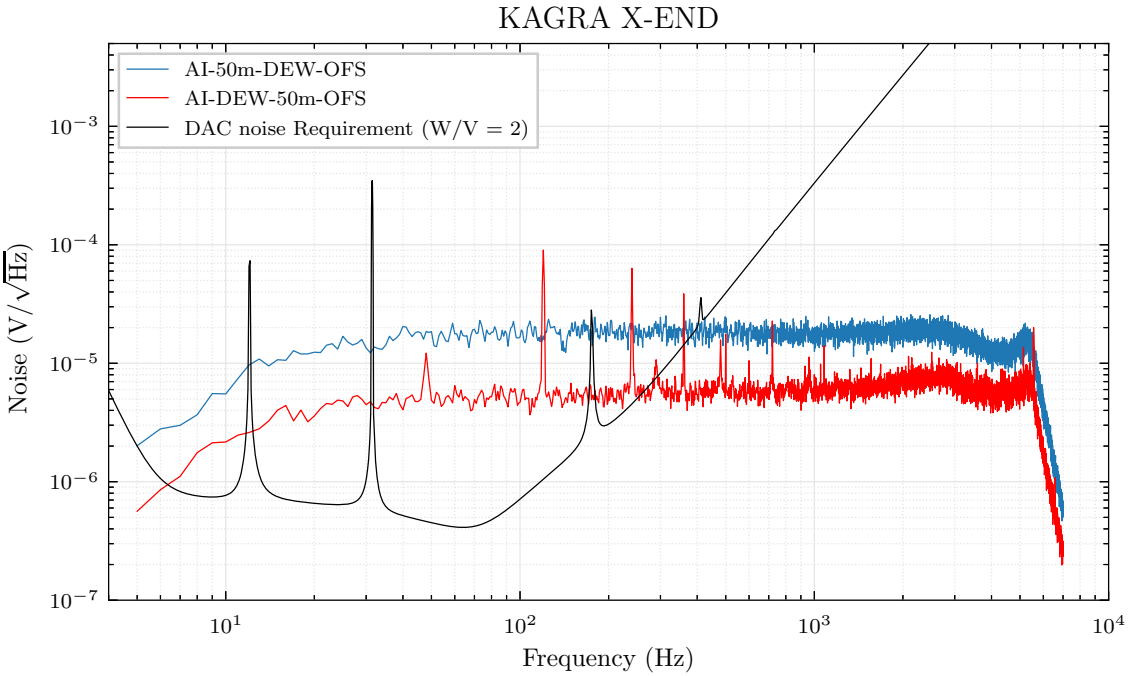

Figure 4.12: The red line and the blue line are measured when De-whitening is located at Place A and Place B in Fig. 4.5 respectively.

Fig. 4.12 shows that if we install our De-Whitening filter at Place B in Fig. 4.5, we got a higher noise floor. The similar effect has been observed in Fig. 4.10.

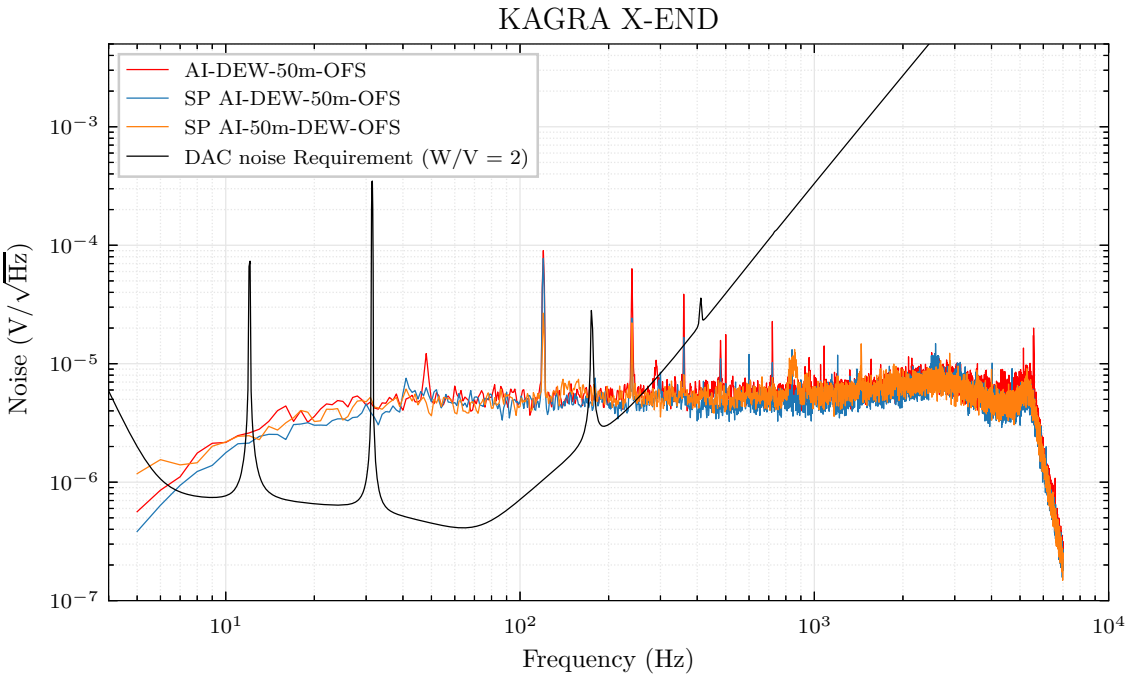

Figure 4.13: Lines labeled with "SP" were measured when we supplied digital system, De-Whitening filter and PCal with Same Power source located in digital system rack.

When we supply our PCal with the shared power source in the digital system rack, the noise floors become independent of the location of De-Whitening filter as you can observe in Fig. 4.13. They are also coincident with the red line in the plot. Among measurements we have tried, whenever the De-Whitening filter is supplied by the same power source as Anti-Image chassis, which is the upstream device of De-Whitening filter, the noise floor we get becomes the same as the red line in Fig. 4.13.

Chapter 5

Validation of Injection Channel

Without loss of generality, We injected binary blackhole signals to test performance of our De-Whitening Filter. Unfortunately, at this moment, we couldn't find a compatible data-taking system with desired noise level and dynamical range to faithfully reconstruct or estimate the expect End-Test Mirror (ETM) displacement that generated by our Photon Calibrator. The reason is that the ADC we used has much larger noise than DAC we used. If we amplify the signal before ADC, as what we did for noise measurement in last chapter, some part of injected waveform can easily saturate ADC.

Besides, We have tried to inject Sine-Gaussian signals. Noise measurement around 100Hz the noise should below the IFO sensitivity Transfer Function measurement above 1kHz performance time delay of excitation channel (absolute timing measurement?) Distortion of Scientific Signal BBH BNS post merger

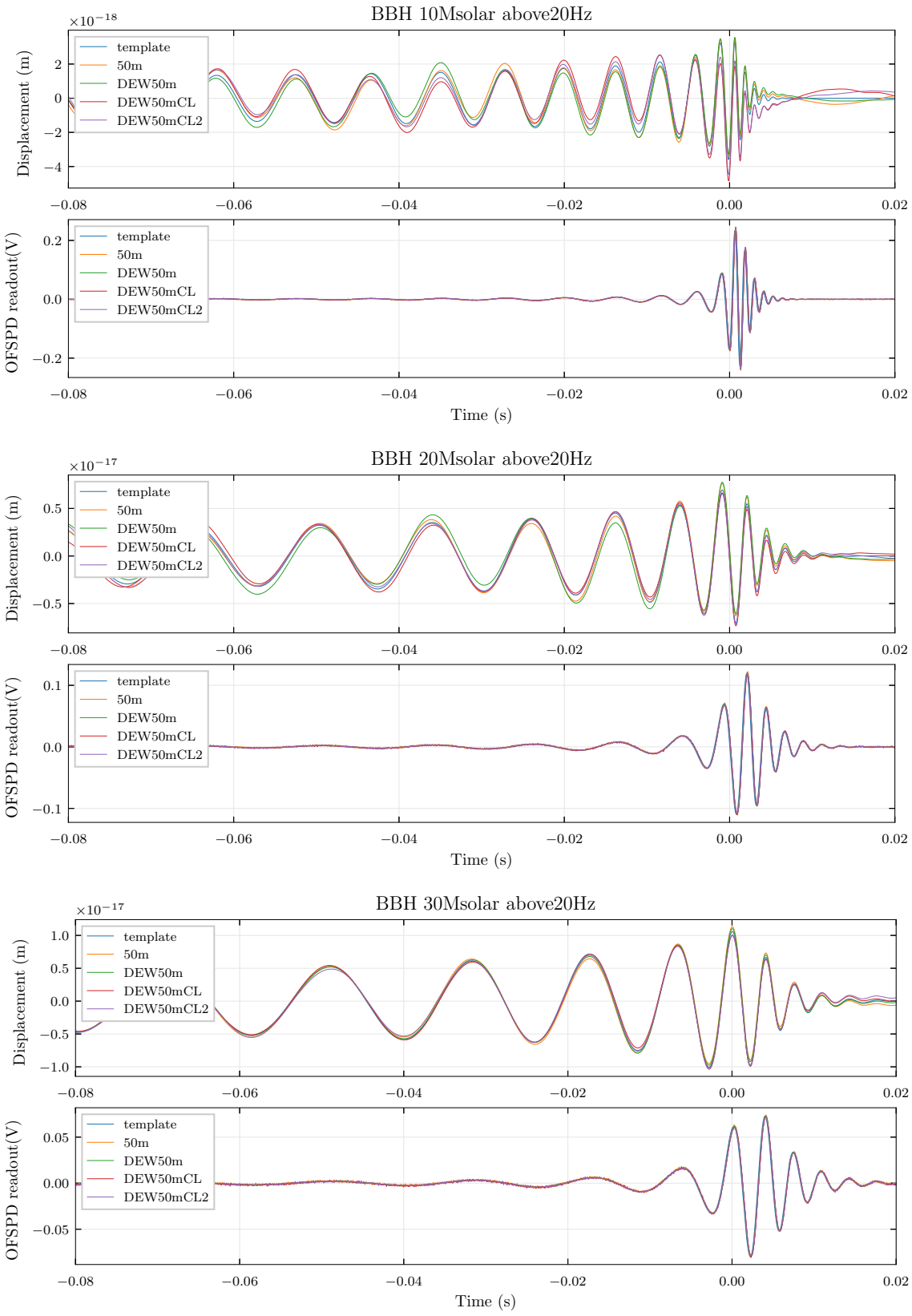

Figure 5.1: Injected Binary Blackhole Merger Signal

Chapter 6

Discussion and Future Works

Although the De-Whitening Filter can attenuate low frequency noise and effectively increase low frequency signal resolution, it limits the maximum excitation signal that can be sent to Photon Calibrator. This is one of intrinsic disadvantages of the De-Whitening filter. In Fig.6.1 we estimated how much dynamical range will be sacrificed.

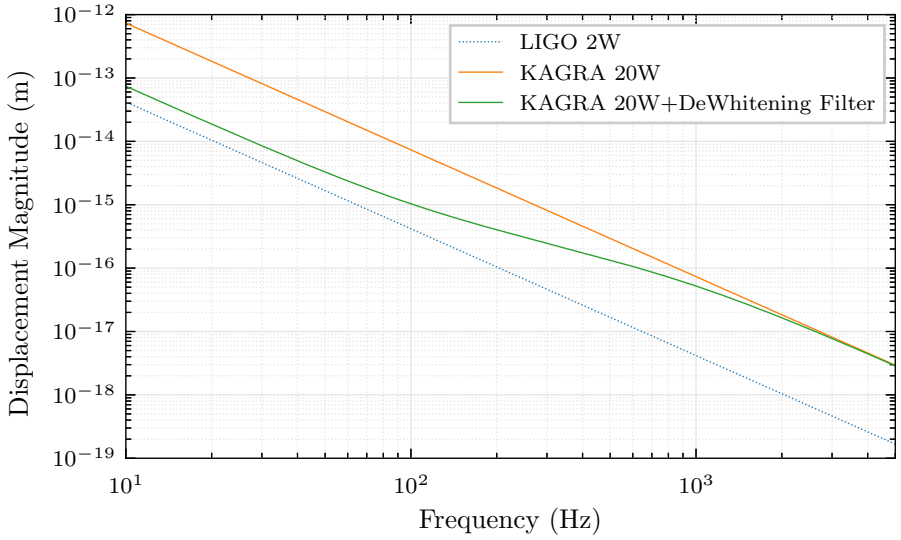

Figure 6.1: Maximum Injection Capability. This is the maximum, assuming 100 percent optical efficiency, displacement of ETM could be generated by Photon Calibrator. It proportional to $1/f^2$ due to the force-to-displacement transfer function of suspended ETM. The green line indicate the maximum laser intensity modulation amplitude that is attenuated by De-Whitening filter.

For the quantization noise from DAC, one can adopt the so-called *Noise Shaping* algorithm [19] to move the low frequency noise to the higher frequency regime, which will be removed by an anti-image filter before it comes into our PCal. Although it cannot increase the low frequency signal resolution that limited by DAC bit-depth, it dose not compromise maximum signal amplitude. As long as it is an approach independent approach to decrease the noise, we can apply it and De-Whitening filter at the same time if necessary.

On the other hand, naively, the noise problem can be solved by using a higher bit-depth DAC card. However, DACs with bit-depths higher than 16bits typically suffer from another noise source due to its *Integral Nonlinearity* (ref). Unless we dedicate significant resources into developing such high precision DAC chip and its auxiliary circuit, it might be challenging to find a satisfying commercial product at this moment.

During the experiments, we found that carrying analog signals on 50m long D-sub cables may be problematic because we have such strict noise requirement. Installation of an extra digital control system near our PCal is favored.

We have successfully modulate PCal laser intensity according to several binary blak hole coalescence waveform templates. Once the main KAGRA interferometer start working, we can verify whether the ETM displacement has been generated as we expected. At the same time, will have ability to crosscheck the response of main interferometer, which is the main goal of hardware injection test.

Bibliography

[1] C. Biwer et al. Validating gravitational-wave detections: The advanced ligo hardware injection system. *Phys. Rev. D*, 95:062002, Mar 2017. doi: 10.1103/PhysRevD.95.062002. URL https://link.aps.org/doi/10.1103/PhysRevD.95.062002.

[2] A Einstein. Grundgedanken und Methoden der Relativitätstheorie, in ihrer Entwicklung dargestellt. Fundamental Ideas and Methods of the Theory of Relativity, Presented in Their Development, after 22 Jan 1920. 1920. URL https://einsteinpapers.press.princeton.edu/vol7-trans/129.

[3] Daniel Kennefick. Einstein versus the physical review. *Physics Today*, 58(9):43–48, 2005. doi: 10.1063/1.2117822. URL https://doi.org/10.1063/1.2117822.

[4] A. Einstein and N. Rosen. On gravitational waves. *Journal of the Franklin Institute*, 223(1):43 – 54, 1937. ISSN 0016-0032. doi: https://doi.org/10.1016/S0016-0032(37)90583-0. URL http://www.sciencedirect.com/science/article/pii/S0016003237905830.

[5] R. A. Hulse and J. H. Taylor. Discovery of a pulsar in a binary system. *ApJ*, 195:L51–L53, January 1975. doi: 10.1086/181708.

[6] J. H. Taylor and J. M. Weisberg. A new test of general relativity - Gravitational radiation and the binary pulsar PSR 1913+16. ApJ, 253:908–920, February 1982. doi: 10.1086/159690.

[7] Joseph H. Taylor. Binary pulsars and relativistic gravity. *Rev. Mod. Phys.*, 66:711–719, Jul 1994. doi: 10.1103/RevModPhys.66.711. URL https://link.aps.org/doi/10.1103/RevModPhys.66.711.

[8] B. P. Abbott et al. Observation of gravitational waves from a binary black hole merger. *Phys. Rev. Lett.*, 116:061102, Feb 2016. doi: 10.1103/PhysRevLett.116.061102. URL https://link.aps.org/doi/10.1103/PhysRevLett.116.061102.

[9] M. Maggiore and Oxford University Press. *Gravitational Waves: Volume 1: Theory and Experiments*. Gravitational Waves. OUP Oxford, 2008. ISBN 9780198570745. URL https://books.google.com.tw/books?id=AqVpQgAACAAJ.

[10] Malik Rakhmanov. Response of test masses to gravitational waves in the local lorentz gauge. *Phys. Rev. D*, 71:084003, Apr 2005. doi: 10.1103/PhysRevD.71.084003. URL https://link.aps.org/doi/10.1103/PhysRevD.71.084003.

[11] DA Clubley, GP Newton, KD Skeldon, and J Hough. Calibration of the glasgow 10 m prototype laser interferometric gravitational wave detector using photon pressure. *Physics Letters A*, 283(1-2):85–88, 2001.

[12] S. Karki et al. The advanced ligo photon calibrators. *Rev. Sci. Instrum.*, 87: 114503, 2016.

[13] H P Daveloza, M Afrin Badhan, M Diaz, K Kawabe, P N Konverski, M Landry, and R L Savage. Controlling calibration errors in gravitational-wave detectors by precise location of calibration forces. *Journal of Physics: Conference Series*, 363(1):012007, 2012. URL http://stacks.iop.org/1742-6596/363/i=1/a=012007.

[14] Rolf Bork. Advligo cds design overview. *LIGO Document Control Center*, (Report No. T0900612), 2010. URL https://dcc.ligo.org/LIGO-T0900612/public.

[15] J. Heefner R. Abbott. Advanced ligo anti-aliasing and anti-image filter function. *LIGO Document Control Center*, (Report No. T070038), 2007. URL https://dcc.ligo.org/LIGO-T070038/public.

[16] R. Bork and A. Ivanov. Advligo cds realtime sequencer software. *LIGO Document Control Center*, (Report No. T0900607), 2012. URL https://dcc.ligo.org/LIGO-T0900607/public.

[17] R. Bork. Real-time code generator (rcg) software component overview. *LIGO Document Control Center*, (Report No. T1200291), 2012. URL https://dcc.ligo.org/LIGO-T1200291/public.

[18] A. Ivanov R. Bork, M. Aronsson. Advligo cds realtime code generator (rcg) application developer's guide. *LIGO Document Control Center*, (Report No. T080135), 2013. URL https://dcc.ligo.org/LIGO-T080135/public.

[19] Ayush Pandey, Christopher Wipf, Rana Adhikari, and Jameson Graef Rollins. Quantization noise in advanced ligo digital control systems. *LIGO Document Control Center*, (Report No. T1500351), 2015. URL https://dcc.ligo.org/LIGO-T1500351/public.